Electro-optic holography method for determination of surface shape and deformation

Cosme Furlong and **Ryszard J. Pryputniewicz**
Center for Holographic Studies and Laser μmechaTronics
Mechanical Engineering Department
Worcester Polytechnic Institute
Worcester, Massachusetts 01609-2280

ABSTRACT

Current demanding engineering analysis and design applications require effective experimental methodologies for characterization of surface shape and deformation. Such characterization is of primary importance in many applications, because these quantities are related to the functionality, performance, and integrity of the objects of interest, especially in view of advances relating to concurrent engineering. In this paper, a new approach to characterization of surface shape and deformation using a simple optical setup is described. The approach consists of a fiber optic based electro-optic holography (EOH) system based on an infrared, temperature tuned laser diode, a single mode fiber optic directional coupler assembly, and a video processing computer. The EOH can be arranged in multiple configurations which include, the three-camera, three-illumination, and speckle correlation modes. In particular, the three-camera mode is described, as well as a brief description of the procedures for obtaining quantitative 3D shape and deformation information. A representative application of the three-camera EOH system demonstrates the viability of the approach as an effective engineering tool. A particular feature of this system and the procedure described in this paper is that the 3D quantitative data are written to data files which can be readily interfaced to commercial CAD/CAM environments.

Keywords: CAD/CAM environment, deformation measurements, electro-optic holography, fiber optics, shape measurements.

1. INTRODUCTION

Traditional engineering design procedures can no longer be applied on current engineering design and analysis applications. Especially, when new and more demanding applications have to be developed in relatively short periods of time while satisfying design objectives, as well as cost and manufacturability. In addition, reliability and durability must be taken into consideration. As a consequence, effective engineering methodologies should be applied in the study and optimization of mechanical and electro-mechanical components[1]; this is known as *concurrent engineering*.

Concurrent engineering can be viewed as a systematic approach to the integrated, concurrent design and analysis of a product and its related processes[2]. This approach is intended to cause the analyst and designer to consider all aspects in the product life cycle from conception, through analysis, optimization, use, service, to disposal, including quality, cost, schedule, and user requirements. Concurrent engineering has the desired features that current demanding engineering applications require. When appropriately applied, the concurrent engineering promotes integration of different engineering disciplines, which naturally produces compatible data between different engineering fields, and therefore, resulting in robust engineering analysis and design products at reduced cycle times and costs.

Determination of shape and deformations/displacements is a very important issue in many applications involving concurrent engineering, because they are directly related to the functionality, performance, and integrity of the object of interest. Characterization of shape can be applied to many areas which include, generation of CAD models from existing samples, or to study of shape changes and wear, whereas determination of deformations/displacements can be related to

strains and/or to rigid body motions and rotations. Shape and deformation can effectively be determined with quantitative optical techniques since they can provide with noninvasive, full field of view information about the object of interest subjected to realistic loading and boundary conditions.

For certain applications, determination of surface shape and deformation using the same experimental setup is required. In addition, it is also required that the experimentally obtained data be compatible with other engineering analysis tools, e. g., CAD/CAE software. In this paper, an electro-optic holography (EOH) system capable of providing 3D surface shape and deformation data is described. The EOH system can be arranged in multiple configurations which include, the three-camera, three-illumination, and speckle correlation modes. In particular, the EOH arranged in the three-camera mode is described. This particular mode is a new approach to determination of surface shape and deformation using optical techniques and has direct benefit to concurrent engineering applications.

2. DESCRIPTION OF THE 3-CAMERA SYSTEM

The EOH has been successfully applied to different fields of nondestructive testing of mechanical components[1,3,4]. Being noninvasive and providing qualitative and quantitative full field information are some of the main advantages of the EOH over other experimental techniques. In addition, it requires much less mechanical stability than that required in conventional holographic interferometry. With the EOH, it is possible to perform static and dynamic investigations of mechanical components subjected to a large variety of loading conditions. Furthermore, it is also possible to measure the shape of mechanical components using optical contouring. Combination of these capabilities makes the EOH a powerful engineering tool that can be effectively utilized to study and optimize mechanical components[1]. Recent technological advances in computer and fiber optic technologies have been applied to the EOH system. These advances have dramatically increased the versatility of the EOH method and have added the possibility of using it in on-site investigations in order to study and diagnose problems in industrial environments.

Figures 1 to 3 depict the major components of a currently operational EOH system used for characterization of shape and extraction of the deformation/displacement vectors in static and dynamic investigations. The light source is an infrared MOPA (Master Oscillator/Power Amplifier) laser diode (LD) with an operational wavelength centered at 994 nm (at 25 ^{o}C), with thermoelectric cooling capabilities, horizontal linearly polarized output, and driven by the controller LDD, Fig. 1. The output of the LD is directed through a Faraday optical isolator (OI) providing back reflection isolation to –41 dB. The OI provides 47^{o} rotation at 994 nm and the polarizer on its input side is set to horizontal polarization in order to match the main polarization axis of the LD output. After the OI, light is lunched into a single mode fiber optic directional coupler assembly, FA (Fig. 2), by means of a fiber coupler (FCA), which is comprised of a GRIN lens, a 5 degrees of freedom stage, and an FC/AP connector port. The main components of the FA are three single mode fiber optic directional couplers (DC1, DC2, DC3), four piezoelectric cylinders (PZT1, PZT2, PZT3, PZT4), and FC connectorized I/O's. Table 1 summarizes the major features of the FA.

Table 1. Major features of the single mode fiber optic directional coupler assembly, FA.

Input port	Application	Mode
I_1	One illumination and three reference beams	Three-camera
I_2	One reference and three illumination beams	Three-illumination
I_2	Four illuminations	Speckle correlation

In the three-camera mode (Fig. 1), the higher output beam from the FA is utilized to illuminate the object of interest (OB) and the lower output beams are used as reference beams. Illumination and reference beams are recombined in the interferometers (IT1, IT2, IT3) and the resultant irradiances transmitted to a video processing computer (IP) using a set of synchronized CCD cameras (CCD1, CCD2, CCD3) providing video frames with resolution of 512x480 pixels and 8-bit in depth. In this configuration, the ceramic piezoelectric cylinder PZT1, Fig. 2, is controlled by the IP and used for phase stepping while PZT2, PZT3, and PZT4, are controlled by the variable phase synthesizer DR and used for quantitative analysis of time-averaged interferograms[4]. This setup occupies a minimum space and can be readily rearranged to obtain different experimental configurations.

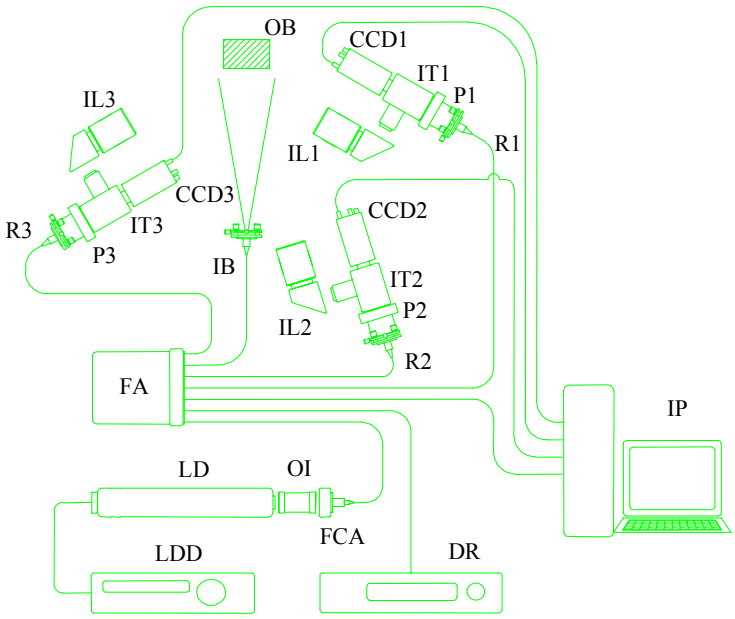

Fig. 1. Fiber optic based EOH system configured in the three-camera mode: LDD is the laser diode driver, LD is the laser diode, OI is the optical isolator, FCA is the fiber coupler, DR is the variable phase synthesizer, IP is the video processing computer, FA is the single mode fiber optic directional coupler assembly, CCD1, CCD2, CCD3 are the cameras, IT1, IT2, IT3 are the interferometers, P1, P2, P3 are the polarizers, IL1, IL2, IL3 are the imaging lenses, R1, R2, R3 are the FC connectorized reference beams, IB is the FC connectorized illumination beam, and OB is the object under investigation.

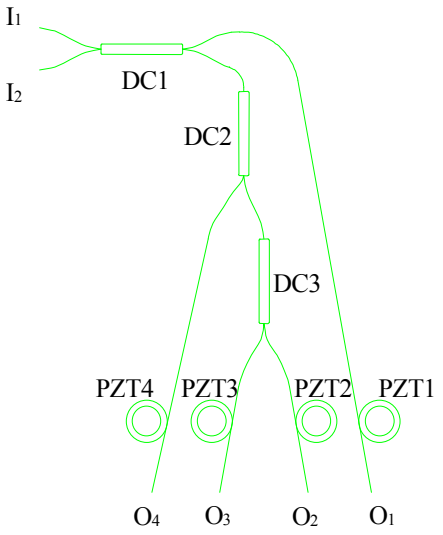

Attenuation, dB

I_1-O_1 = 1.10	I_2-O_1 = 1.10
I_1-O_2 = 10.9	I_2-O_2 = 10.9
I_1-O_3 = 10.9	I_2-O_3 = 10.9
I_1-O_4 = 11.7	I_2-O_4 = 11.7

Splitting, %

I_1	I_2	
80	20	O_1
7	28	O_2
7	28	O_3
6	24	O_4

Fig. 2. Single mode fiber optic based directional coupler assembly (FA): I_1, I_2 are the FC connectorized input fibers, DC1, DC2, DC3 are the directional couplers, PZT1, PZT2, PZT3, PZT4 are the ceramic piezoelectric cylinders, and O_1, O_2, O_3, O_4 are the FC connectorized output fibers.

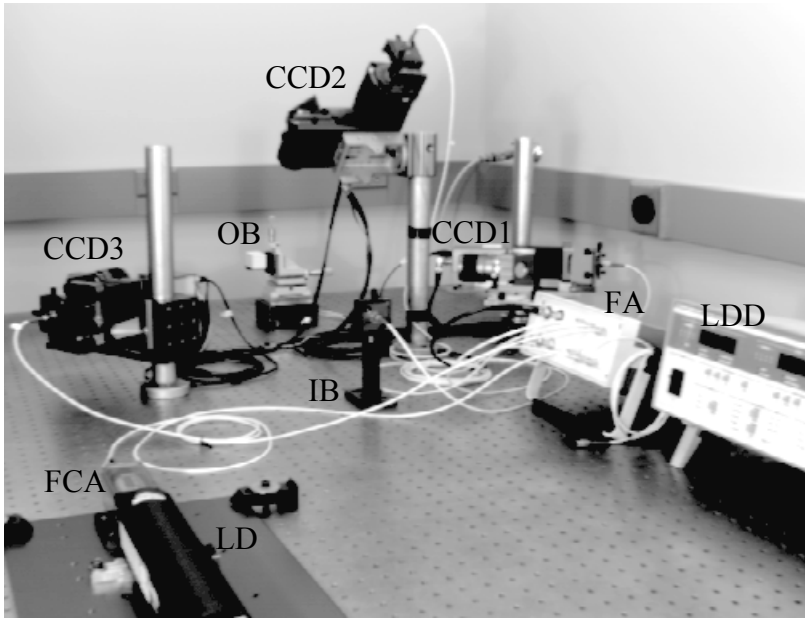

Fig. 3. Fiber optic based EOH system configured in the three-camera mode: LD is the laser diode, LDD is the laser diode driver, FA is the single mode fiber optic directional coupler assembly, FCA is the fiber coupler, IB is the illumination beam, CCD1, CCD2, CCD3 are the cameras, and OB is the object under investigation.

2.1. Static investigations

In the EOH, optical path change, which is related to mechanical deformations/displacements in static investigations, is extracted from the interference pattern of object and reference beams having complex light fields F_o and F_r. After beam splitting, and considering phase stepping, irradiance of the combined wavefronts as recorded by the n-th video frame is described by

$$\begin{aligned} I_n &= (F_o + F_r)(F_o + F_r)^* \quad , \\ &= \left\{A_o \exp\left[-j\left(\phi_o + \theta_n\right)\right] + A_r \exp(-j\phi_r)\right\} \cdot \left\{A_o \exp\left[j\left(\phi_o + \theta_n\right)\right] + A_r \exp(j\phi_r)\right\} \quad , \\ &= {A_o}^2 + {A_r}^2 + 2A_o A_r \cos\left(\Delta\phi + \theta_n\right) \quad , \end{aligned} \tag{1}$$

where A_o and A_r are the amplitudes of the object and reference beams, $\Delta\phi$ is the phase due to the optical path difference between observation and illumination beams, θ_n is the known phase step introduced between the frames[4], and for clarity, plane wavefronts are assumed. To facilitate static investigations, the argument of the periodic term of Eq. 1 is modified to include the phase change due to static deformations/displacements of the object of interest subjected to specific loading and boundary conditions. This phase change is characterized by the fringe-locus function Ω, whose constant values define fringe loci on the surface of the object and observed at point (u,v) of the detector as

$$\Omega(u,v) = 2\pi n(u,v) = \mathbf{K}(u,v) \cdot \mathbf{L}(u,v) \quad , \tag{2}$$

where $n(u,v)$ is the interferometric fringe order at the (u,v) location of the imaging plane, $\mathbf{K}$ is the sensitivity vector, and $\mathbf{L}$ is the displacement vector. Therefore, the irradiance from a deformed object can be described as

$$I_n'(u,v) = I_o(u,v) + I_r(u,v) + 2A_o(u,v)A_r(u,v)\cos\left[\Delta\phi(u,v) + \Omega(u,v) + \theta_n\right] \quad , \tag{3}$$

where I_o and I_r represent the intensities of the object and reference beams (i. e., amplitudes squared), respectively, and I_o is assumed to remain constant during the frame grabbing. Since it is Ω that carries information pertaining to mechanical deformations/displacements, the EOH's video frame processing algorithm eliminates $\Delta\phi$ from the argument of the periodic function of the irradiance distributions given in Eqs 1 and 3, yielding an image that has intensity modulated by a periodic function with Ω as the argument[5].

The EOH can work in display and data mode. In the display mode, interference patterns are observed at video rate speed and are modulated by a cosinusoidal function of the form

$$8 Ao\, Ar \cos\left(\frac{\Omega}{2}\right), \tag{4}$$

which is obtained by performing specific algebraic operations between frames acquired at the two different states of deformation, described by Eqs 1 and 3, respectively. This mode is used for adjusting the EOH system and for qualitative investigations. The data mode is used for performing quantitative investigations. In the data mode, two additional images are generated: a cosinusoidal image,

$$D = 64 A_O^2 A_r^2 \cos(\Omega) \quad , \tag{5}$$

and a sinusoidal image,

$$N = 64 A_O^2 A_r^2 \sin(\Omega) \quad , \tag{6}$$

which are processed simultaneously to produce quantitative results by computing

$$\Omega = \tan^{-1}\left(\frac{N}{D}\right). \tag{7}$$

Figure 4a depicts a typical interferogram obtained with the EOH system functioning in static display mode: a computer CPU fan in the cooling regime after being subjected to a 30 ^{o}C air flow.

2.2. Dynamic investigations

To perform dynamic investigations, or modal analysis, using the EOH, it is necessary to take into consideration a time varying fringe-locus function $\Omega_t\,(u,v,t)$ which is related to periodic motion of the object under investigation[4,6]. Using Eq. 3, it is possible to write

$$I_t(u,v,t) = I_o(u,v) + I_r(u,v) + 2A_o(u,v)A_r(u,v)\cos\left[\Delta\phi(u,v) + \Omega_t(u,v,t)\right] \quad . \tag{8}$$

Since the CCD camera registers average intensity at the video rate characterized by the period Δt which, in the EOH system used in this study, is equal to 1/30-th of a second, the intensity that is observed can be expressed mathematically as

$$I(u,v) = \frac{1}{\Delta t}\int_{t}^{t+\Delta t} I_t(u,v,t)\,dt \quad , \tag{9}$$

and, using phase stepping, the resultant intensity distribution for the n-th frame can be written as

$$I_{t_n}(u,v) = I_o(u,v) + I_r(u,v) + 2A_o(u,v)A_r(u,v)\cos[\Delta\phi(u,v) + \theta_n]M[\Omega_t(u,v)] \quad , \tag{10}$$

where $M\left[\Omega_t(u,v)\right]$ is known as the characteristic function determined by the temporal motion of the object[7]. For the case of sinusoidal vibrations with the period much shorter than the video framing time,

$$M\left[\Omega_t(u,v)\right] = J_o\left[\Omega_t(u,v)\right] \quad , \tag{11}$$

where $J_o\left[\Omega_t(u,v)\right]$ is the zero order Bessel function of the first kind[4]. Equation 10 contains four unknowns: irradiances I_o and I_r, phase difference $\Delta\phi$, and the fringe-locus function Ω_t. The EOH's video frame processing algorithm eliminates $\Delta\phi$ from the argument of the irradiance function given by Eq. 10, using a set of four equations obtained at specific step size value of θ_n. For time-average investigations, the EOH can work in display and data modes. In the display mode, interference patterns are observed at video rate and are modulated by a function of the form

$$4A_oA_r\left|M(\Omega_t)\right| \quad , \tag{12}$$

this mode is used for adjusting the EOH system and for qualitative investigations. Figure 4b shows a typical interferogram, obtained with the EOH system functioning in the time-average display mode: a computer CPU fan loaded at one of its fundamental resonant modes of vibration obtained at 4512 Hz.

The data mode is used for performing quantitative investigations[4]. In the data mode, additional images of the form

$$16I_oI_rM^2(\Omega_t) \quad , \tag{13}$$

are generated for quantitative processing and extraction of Ω_t.

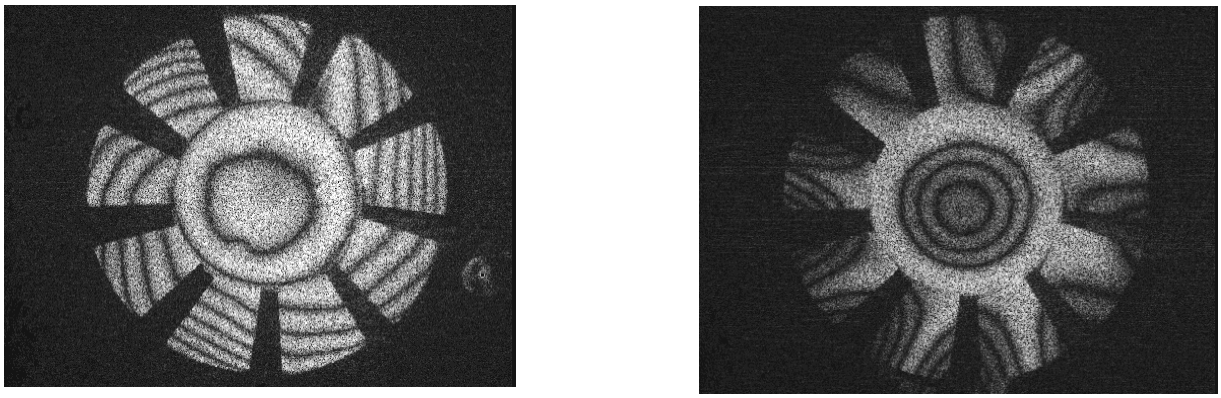

(a) (b)

Fig. 4. EOH applied to static and dynamic investigations of a computer CPU fan: (a) static mode (double-exposure) - cooling regime after being subjected to a 30 ^{o}C air flow, and (b) dynamic mode (time-averaged exposure) - one of the fundamental resonant modes of vibration of the fan observed at 4512 Hz.

2.3. Shape measurements

To determine surface shape using the EOH, the two wavelength technique to generate depth contours related to the geometry of the object under investigation is applied. The wavelength of the LD can be tuned by controlling the temperature of the thermally controlled stage of the MOPA diode, therefore, modifying the optical path length and generating a phase difference, $\Delta\gamma$, which for an specific point on the object P is given by

$$\Delta\gamma = \gamma_2 - \gamma_1 = \frac{2\pi}{\Lambda}\left(\overline{IP} + \overline{PO}\right) \quad , \tag{14}$$

where γ_1 is the phase of the optical path length recorded at the first wavelength, γ_2 is the phase of the optical path length recorded at the second wavelength, $\overline{IP}$ is the distance between the illumination point and point P, $\overline{PO}$ is the distance between P and the observation point, and Λ is the synthetic wavelength given by

$$\Lambda = \frac{\lambda_1 \lambda_2}{\lambda_1 - \lambda_2} \quad . \tag{15}$$

Contouring can be performed by using the EOH in static mode. This is done by acquiring a set of interferograms using wavelength λ_1, representing a reference state, or undeformed state, and then acquiring a second set of interferograms after the wavelength has been changed to λ_2, representing a modified state, or deformed state. The phase change related to depth contours, $\Delta\gamma$, obtained after performing this operation is now equivalent to the fringe-locus function Ω in static investigations, so Eqs 3 to 7 can be applied. Phase information obtained after applying Eq. 7 is a discontinuous wrapped function varying in the interval $(-\pi,\pi)$ and further processing is required in order to obtain a continuous phase distribution by the application of phase unwrapping algorithms.

For practical use of the contouring measurements, it is necessary to characterize the wavelength properties of the laser diode. Temperature tuning for a MOPA diode can be approximated as[8]

$$\lambda = \lambda_o + \frac{d\lambda}{dT}(T - T_o) \quad , \tag{16}$$

where λ is the output wavelength at temperature T, λ_o is the output wavelength at temperature T_o, and $d\lambda/dT$ is the wavelength-temperature tuning slope. λ_o and T_o are given as 994 nm and 25 ^oC, respectively - obtained from the spectral characteristics provided by the laser diode manufacturer. The wavelength-temperature tuning slope is obtained by contouring a gage block of known dimensions, Fig. 5, which provides a value of 0.068 nm/^oC (the laser diode manufacturer suggests a value of 0.07 nm/^oC).

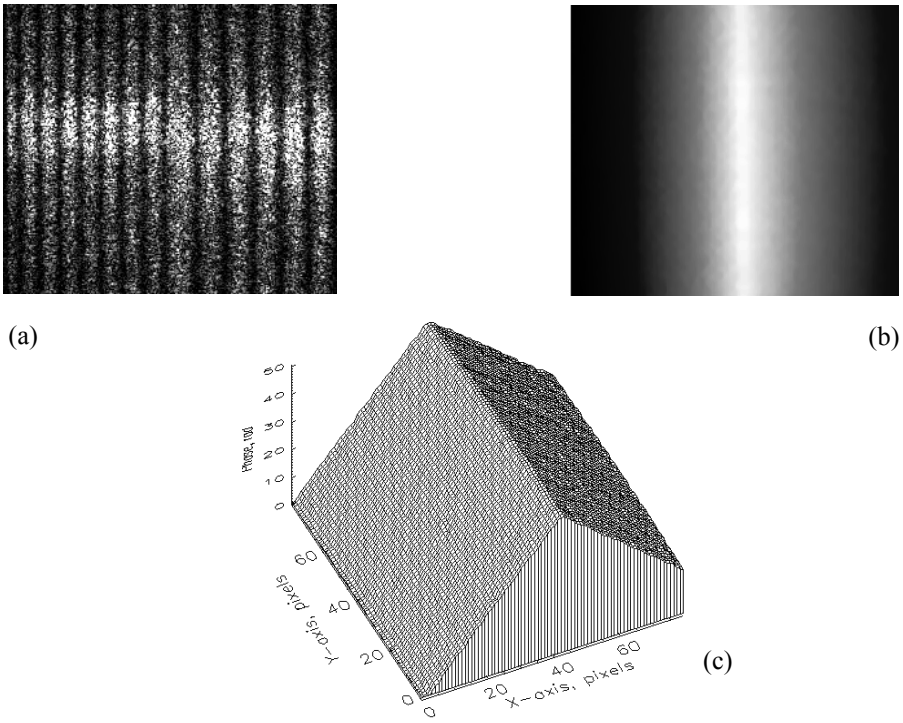

Fig. 5. Laser diode calibration by contouring a gage block: (a) the EOH fringe pattern, (b) unwrapped phase distribution, (c) the EOH determined contour of the gage block.

2.4. Three-cameras mode

With the three-camera system, it is possible to determine surface shape by means of the two-wavelength optical contouring, and deformations/displacements by solution of Eq. 2 for multiple sensitivity vectors[5,7,9]. A major difficulty in the three-camera arrangement is pixel correspondence between images, which allows the full determination of the left-hand side of Eq. 2 from unwrapped phase maps. The following algorithm is proposed as a solution to the pixel correspondence problem:

(a) evaluate the projection perspective matrix with respect to a specific absolute coordinate system,
(b) determine the optical center from the projection perspective matrix, which provides information about the orientation of the camera with respect to the absolute coordinate system - useful in characterizing the sensitivity vector,
(c) contour the surface of interest,
(d) orientate the surface of interest with respect to a plane parallel to the focal plane, and
(e) perform a 2D pixel mapping to a rectangular domain (with same dimensions for each camera) by use of isoparametric shape functions[10].

This procedure is applied to each camera, which results in automatic pixel correspondence between images.

2.4.1. Determination of the projection perspective matrices

Figure 6 depicts the geometrical setup for the three-camera EOH system. The important parameters in this arrangement include the focal and retinal planes, and the corresponding optical axes and optical centers of the cameras.

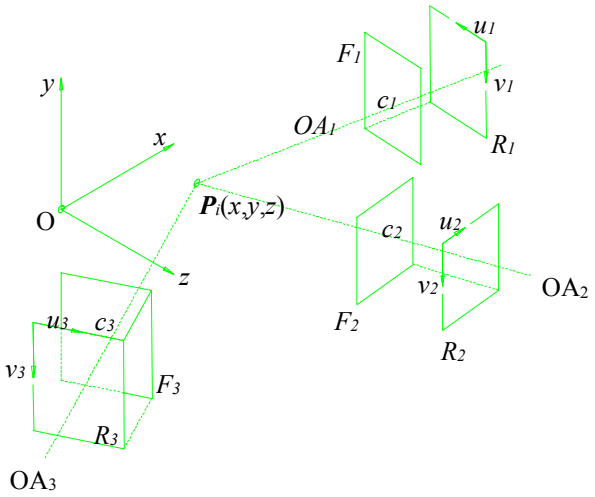

Fig. 6. Three-camera arrangement. c_1, c_2, c_3 are the optical centers of the three cameras, F_1, F_2, F_3 are the focal planes, R_1, R_2, R_3 are the retinal planes, OA_1, OA_2, OA_3 are the optical axes, (u_1,v_1), (u_2,v_2), (u_3,v_3), are the origins of retinal planes, O is the origin of the absolute coordinate system, and point $P_i(x,y,z)$ is the i-th point on the object of interest.

Each camera registers the projection of 3D points in space onto their corresponding retinal planes. This projection can be represented, for each camera, by the following transformation:

$$\boldsymbol{m} = \boldsymbol{Q} \cdot \boldsymbol{P} \quad , \tag{17}$$

with $\boldsymbol{m}$ being a vector containing retinal pixel coordinates (u,v), $\boldsymbol{Q}$ the transformation matrix (projection perspective matrix), and $\boldsymbol{P}$ a vector containing 3D coordinates. Equation 17 can be written as

$$\begin{pmatrix} U \\ V \\ S \end{pmatrix}_i = \begin{pmatrix} q_{11} & q_{12} & q_{13} & q_{14} \\ q_{21} & q_{22} & q_{23} & q_{24} \\ q_{31} & q_{32} & q_{33} & q_{34} \end{pmatrix} \begin{pmatrix} x \\ y \\ z \\ 1 \end{pmatrix}_i = \begin{pmatrix} \boldsymbol{q}_1^T & q_{14} \\ \boldsymbol{q}_2^T & q_{24} \\ \boldsymbol{q}_3^T & q_{34} \end{pmatrix} \boldsymbol{P}_i \quad , \tag{18}$$

where $u=U/S$, $v=V/S$, and S is a scale factor, q_{jk} are the components of the transformation matrix $\boldsymbol{Q}$, and $(x,y,z)_i$ is the i-th 3D point $\boldsymbol{P}_i$. By further reformulation, it is possible to write Eq. 18 as

$$\begin{pmatrix} x_i & y_i & z_i & 1 & 0 & 0 & 0 & 0 & -u_i x_i & -u_i y_i & -u_i z_i & -u_i \\ 0 & 0 & 0 & 0 & x_i & y_i & z_i & 1 & -v_i x_i & -v_i y_i & -v_i z_i & -v_i \\ . & . & . & . & . & . & . & . & . & . & . & . \\ . & . & . & . & . & . & . & . & . & . & . & . \end{pmatrix} \cdot$$

$$\begin{pmatrix} q_{11} & q_{12} & q_{13} & q_{14} & q_{21} & q_{22} & q_{23} & q_{24} & q_{31} & q_{32} & q_{33} & q_{34} \end{pmatrix}^T = \boldsymbol{0} \quad , \tag{19}$$

which is a system of equations of the form $\boldsymbol{A}\cdot\boldsymbol{q}=\boldsymbol{0}$, with $\boldsymbol{A}$ being an N x M matrix of rank 11, $\boldsymbol{q}$ being an unknown vector containing the components of the transformation matrix, and $\boldsymbol{0}$ being the null vector. In order to solve Eq. 19, it is necessary to impose constrains on the system of equations in order to assure that convergence to the trivial solution is avoided (i. e., $\boldsymbol{q}=\boldsymbol{0}$), which has no physical significance. Constraints are determined by studying the mathematical properties of matrix $\boldsymbol{Q}$ and are identified to be $||\boldsymbol{q}_3||^2 = 1$, and $(\boldsymbol{q}_1 \wedge \boldsymbol{q}_3) \cdot (\boldsymbol{q}_2 \wedge \boldsymbol{q}_3) = 0$, indicating an orthogonal matrix. Once the matrix $\boldsymbol{Q}$ has been calculated after application of numerical analysis and constrained optimization methods[11], the optical center of a camera can be determined.

2.5. Representative application

Figures 7 to 12 summarize a representative application of the three-camera EOH system. The sample utilized is a flat milled aluminum block of dimensions 25.4 x 25.4 x 50.8 mm^3. The sample had white diffuse surface finish and reference marks attached to four of its surfaces. Figure 7 shows views of the object as well as origins of camera and absolute coordinate system. Coordinates of the marks (centroids) were digitized and measured with respect to the identified absolute coordinate system. The object was mounted on a precision stage and placed for investigation in the EOH setup, Fig. 3.

Once in the experimental setup, the cameras were orientated and calibrated. The orientation was performed according to procedures developed in the course of this study. Calibration consisted of performing an automatic identification of the marks and corresponding centroids with respect to the retinal planes of the cameras. After identification and localization, the projection perspective matrices for each camera were calculated, as well as the position of their optical centers with respect to the absolute coordinate system. In addition, intrinsic and extrinsic parameters of each camera were also calculated from the projection perspective matrix (i. e., magnification factors, distortion, etc). Figure 8 depicts one of the intermediate results obtained while performing an automatic identification of the marks and localization of their corresponding centroids.

Contouring was performed on one of the front surfaces of the sample. Figure 9 shows the interference patterns that were observed. Surface shape was obtained after averaging the determined shapes from each camera (bilinear isoparametric shape functions were applied[12] for performing pixel correspondence between images, Fig. 10). Correction for phase curvature was applied by utilization of Eq. 14 for known positions of observation and illumination.

After contouring, the sample was subjected to a rigid-body motion loading. Figures 11 and 12 show the corresponding observed interference patterns and the quantified components of deformation obtained by solving Eq. 2 for three sensitivity vectors.

Quantitative data obtained for surface shape and deformation, as shown in Figs 9 and 12, is written to .ibl (imported blend) files, which can be readily read in CAD environments[13] for further manipulation and application in hybrid experimental and computational investigations[1].

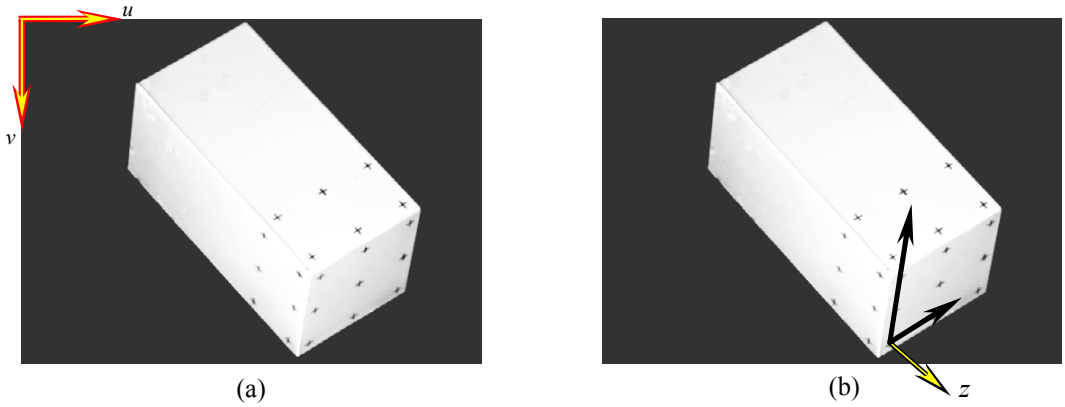

Fig. 7. Calibration block containing 27 marks of known (x,y,z) coordinates (centroids). Perspective views showing: (a) origin of camera coordinate system (in the upper left-hand corner of the picture), (b) selected origin of absolute coordinate system located on the surface of interest - coinciding with one of the marks.

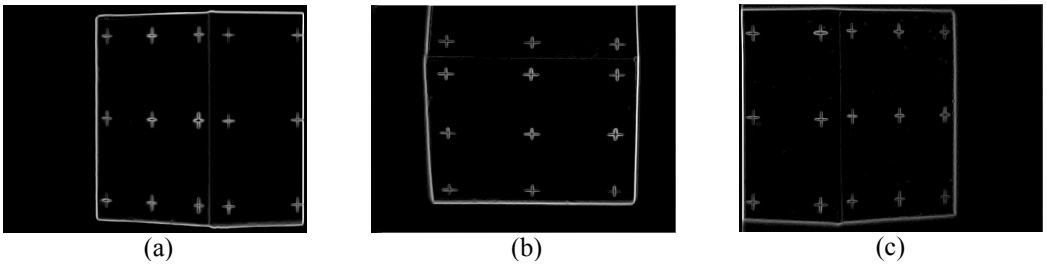

Fig. 8. Automatic determination of pixel coordinates $(u,v)_i$ for each mark (centroids) on the calibration block: (a) as observed from camera CCD1, (b) camera CCD2, (c) and camera CCD3.

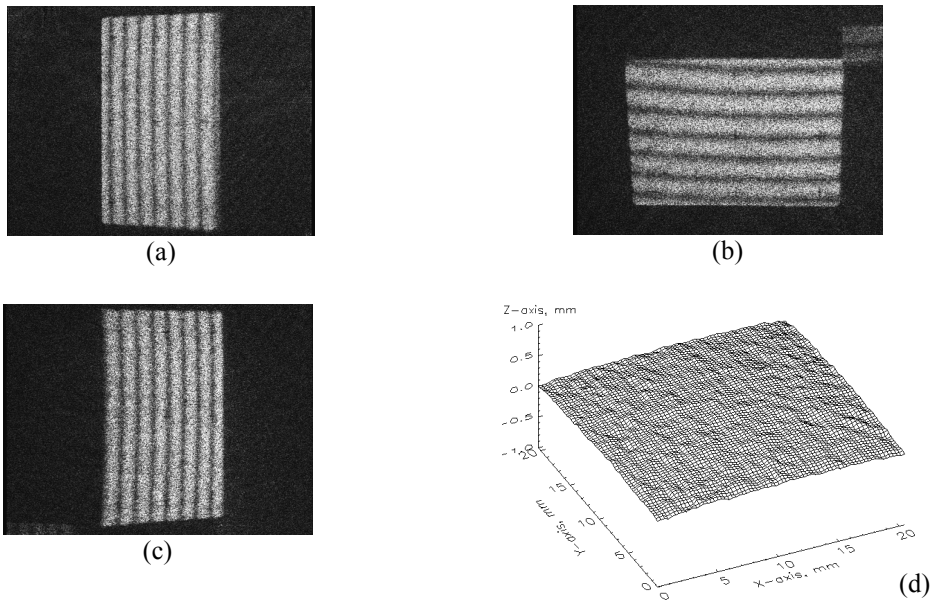

Fig. 9. Contouring the surface of interest on the calibration block, $\lambda_l = 993.73$ nm, $\Delta T = 5$ °C: (a) as observed from camera CCD1, (b) camera CCD2, (c) camera CCD3, (d) determined contour.

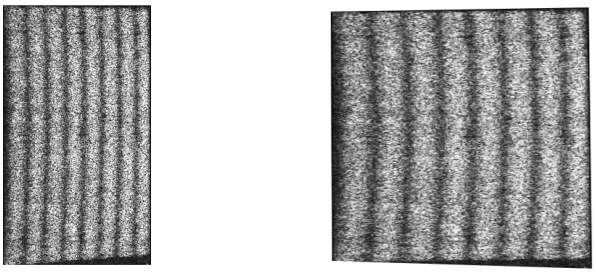

(a) (b)

Fig. 10. Typical 2D pixel mapping using isoparametric shape functions: (a) area of interest as observed from camera CCD3, (b) transformed image. Identified marks are used as reference during the transformation.

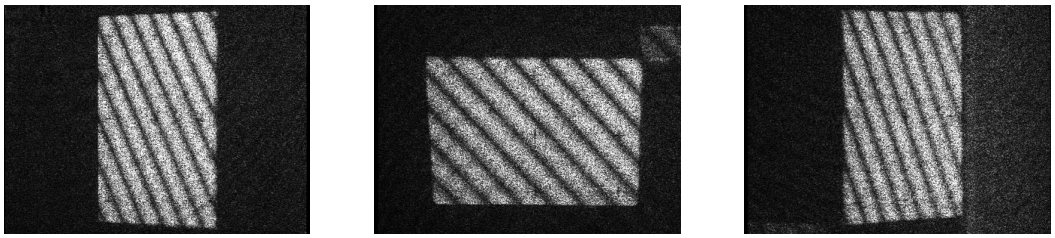

(a) (b) (c)

Fig. 11. Calibration block subjected to rigid-body motion. Observed interference patterns on the surface of interest from: (a) camera CCD1, (b) camera CCD2, (c) camera CCD3.

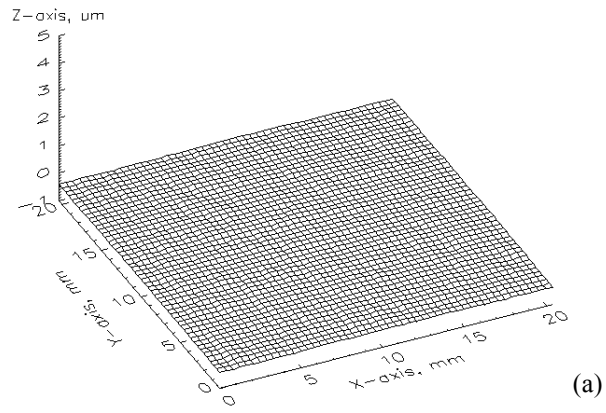

(a)

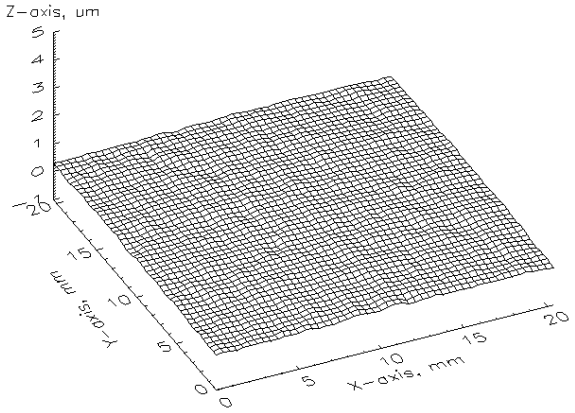

(b)

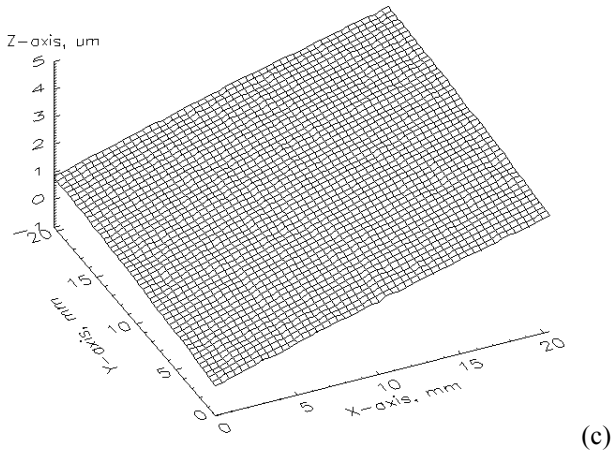

(c)

Fig. 12. Evaluation of the displacement components corresponding to interferograms shown in Fig. 11: (a) *x*-component, (b) *y*-component, (c) *z*-component.

3. CONCLUSIONS AND FUTURE WORK

A fiber optic based EOH system for determination of 3D surface shape and deformation has been described. The EOH can be arranged in three possible modes: the three-camera, three-illumination, and speckle correlation. The three-camera mode was described in this paper as well as a brief description of the methodologies used for extraction of quantitative 3D data. In addition, a representative example is shown. The three-camera, fiber optic based EOH system, is a new technique, and as such, characterization of its performance and applicability are new tasks. These tasks are of current interest and constitute a part of future developments of this technique.

4. ACKNOWLEDGEMENTS

The authors would like to thank Dr. John Hanlon for all of his support in this project. Thanks are also to Mr. Peter Hefti for his valuable discussions and assistance.

5. REFERENCES

1. C. Furlong and R. J. Pryputniewicz, "Hybrid, experimental and computational, investigation of mechanical components," *Proc. SPIE*, 2861:13-24, 1996.

2. D. Gerwin and G. Susman, "Special issue on concurrent engineering," *IEEE Transactions on Engineering Management*, 43(2):118-123, 1996.

3. R. J. Pryputniewicz, "A hybrid approach to deformation analysis," *Proc. SPIE*, 2342:282-296, 1994.

4. R. J. Pryputniewicz and K. A. Stetson, "Measurement of vibration patterns using electro-optic holography," *Proc. SPIE*, 1162:456-467, 1989.

5. R. J. Pryputniewicz, "Quantitative determination of displacements and strains from holograms," Ch. 3 in P. K. Rastogi, ed., *Holographic interferometry*, Springer-Verlag, Berlin, pp. 33-72, 1994.

6. T. W. Bushman, *Automated fringe unwrapping by energy minimization*, MS Thesis, Worcester Polytechnic Institute, Worcester, MA, 1993.

7. C. M. Vest, *Holographic interferometry*, Wiley, NY, 1979.

8. *Laser diode operator's manual and technical Notes*, SDL, Inc., San Jose, CA, 1994.

9. Yu. I. Ostrovsky, V. P. Shchepinov, and V. V. Yakovlev, *Holographic interferometry in experimental mechanics*, Springer-Verlag, Berlin, 1991.

10. M. A. Celia and W. G. Gray, *Numerical methods for differential equations*, Prentice-Hall, Englewood Cliffs, NJ, 1992.

11. G. H. Golub and C. F. Van Loan, *Matrix computations*, The Johns Hopkins University Press, Baltimore, MD, 1989.

12. *IDL Reference Guide*, Research Systems, Inc., Boulder, CO, 1997.

13. *Pro/Engineer. Release Notes. v. 20*, Parametric Technology Corporation, Waltham, MA, 1998.